6. FRET-based glucose sensor

In this Chapter protein ligand interactions will be discussed for the case of glucose interacting with a FRET-based genetically created biosensor. In the previous Chapter 5 the focus was on the dynamic and thermodynamic aspects of the binding, whereas in this Chapter the structural aspects will be discussed in more detail. The sensors discussed here are expected to work by structural reorientation or reorganisation, two very common aspects in biosensor signal transfer.[25, 87] To this purpose the concept of genetically encoded biosensors will be introduced in Section 6.1, how they are constructed and what similarities they have to naturally occurring biosensors. Then the specific sensor constructs analysed in Section 6.2 and the results obtained from SAXS experiments performed on them, Section 6.3 will be presented. This data will then be analysed by fitting different models to them.

6.1. Genetically encoded biosensors

Biosensors are generally understood to be molecules or cells that are sensitive to specific compounds or processes in living organisms.[88, 89] This sensitivity usually leads to a signal transfer or conformational change. The main difference between genetically encoded and naturally occurring biosensors is that the former are created in the lab for a specific purpose.[13, 90] In both cases a specific binding site, with which the targeted ligand interacts, exists. However, in the case of genetically encoded biosensors these binding sites consist of specifically selected biosensors. These sensors are chosen for their interaction with the ligand the artificial sensor will be created for. By attaching a dye,

or a FP to the biosensor, which becomes the genetically encoded sensors binding site, the signal transfer is artificially altered, with the aim to increase it. These attachments may also alter the strength of the ligand binding.[13, 20, 89] Here the focus will be on biosensors which create fluorescent signals. For the simplest case of FRET signal transfer a change in the distance between two different coloured dies is sufficient.[26] However, if FPs are used the flurophore has a dipole structure and therefore both a change in distance, as well as a change in relative chromophore orientation, or both can cause the signal transfer.[18]

So far the general approach has been that a binding site, which suits the interactions required, is chosen, as well as structure or linker to link the binding site to signalling units.[13, 89, 90] These were then optimised by a combination of trial and error and pick and mix approaches.[18] In the first approach a general linking is performed, which is then mutated until the sensor is optimised. By observing which effects appear to be more promising, or making assumptions about how to increase efficiency the most efficient sensors are selected. This approach is best described an iterative mutation process.

The aim of this analysis is to form a hypothesis that adequately describes why different sensor models obtained from such an iterative approach differ in their efficiency. It is important to be able to link the structural behaviour of a sensor to its efficiency. An understanding of the structural properties and their causes of a good sensor compared to a bad one would aid in the optimisation of sensor design.

6.2. Analysed constructs of glucose biosensors

In this Section a group of sensors chosen for a closer study will be introduced. The sensor constructs selected are FRET-based glucose biosensors, which were already analysed in regards of their different FRET efficiency in relation to the structure chosen.[12, 13] In Fig. 6.1 the different glucose sensor constructs created in the group of Martina Pohl (FZ Jülich IBG-1) are shown, along with the analysis done on them.[12, 13]

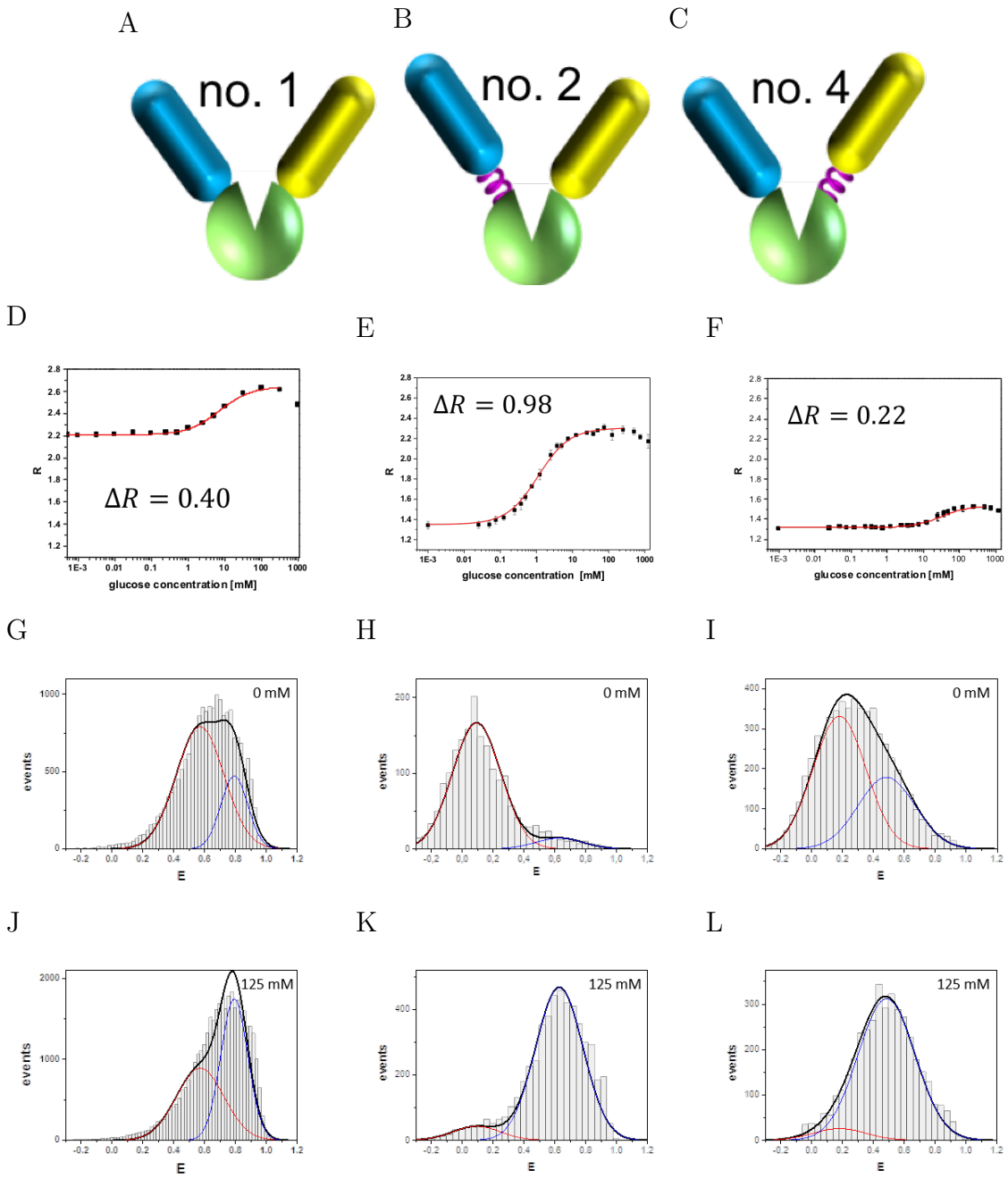

Figure 6.1.: *Sketches of the different sensor constructs analysed with smFRET by Henning Höfig, the change in FRET energy transfer for added glucose is shown in the titration curves. ΔR can be used as an indicator of sensor efficiency. The larger the value is, the more efficient the sensor. A, B, and C show sketches of the different sensor constructs. Below the sensor the corresponding titration curve is shown in D, E, F. Under these the smFRET (single molecule FRET) measurements performed for each sensor are shown. Here G, H, and I show the smFRET measurements without added glucose and J, K, and L those with added glucose.[12]*

All sensors consist of a glucose binding protein (Glc-BP), to which two FPs (mTurquoise, Venus) are attached, see Fig. 6.2. The amino acid sequences for the sensors chosen for closer analysis are given in Appendix D. To attach the FPs to the Glc-BP a flexible linker was used, which does not have the potential to form a secondary structure.[13] From the data given in Fig. 6.1 it can be observed that the presence or absence of a linker at the C-terminal FP (mTurquoise) has a relevant effect on the sensor efficiency. Sensor 1 was selected as a reference for a linker free construct. Sensor 2 is the most efficient sensor and has a C-terminal linker, whiles sensor 4 has the opposite linker positioning with no C-terminal linker, but an N-terminal linker and is the least efficient.

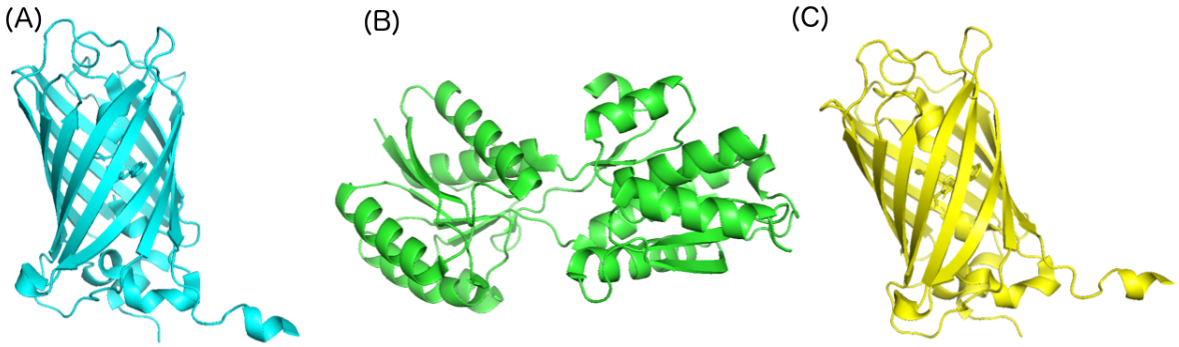

Figure 6.2.: *A shows the crystal structure of mTurquoise, B the crystal structure of the glucose binding protein and C the crystal structure of Venus. These components were artificially connected in order to create the FRET-sensitive glucose sensors.*

$$E = \frac{1}{\left(1 + \frac{R_{DA}}{R_0}\right)^6} \tag{6.1}$$

$$R_0 = 0.221 \cdot (\kappa^2 \cdot QD \cdot n^{-4} \cdot J)^{\frac{1}{6}} \tag{6.2}$$

$$R = \frac{I_{DA}}{I_D} \tag{6.3}$$

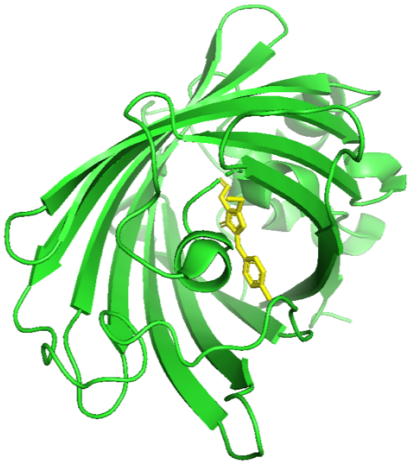

Figure 6.3.: *Crystal structure of GFP with the chromophore shown in yellow, the chromophore is the dipole structure which is relevant for the FRET signal*

$$E = 1 - R \tag{6.4}$$

Having briefly introduced the different sensor constructs and the sensors selected a short overview of the relevant parameters for FRET will be given. In Fig. 6.3 the position of the chromophore is shown for the green fluorescent protein, however it is the same for all FPs.[91] The fluorescent properties of the FPs are used both to observe the change in glucose concentration by tracking the fluorescent intensities in application and during analysis. For FRET the donor chromophore is excited and can then transfer this energy from its excited state to the acceptor chromophore via dipole-dipole coupling.[92] The efficiency of this transfer is measured, since the chromophores are dipoles the efficiency depends on the angle between donor and acceptor dipole, the distance, or more likely a combination of the two, see Eq. 6.1.[93] Here E is the FRET efficiency, R_{DA} the distance between the centres of mass for the dipoles and R_0 is the Förster radius described in Eq. 6.2.[93] The FRET efficiency E is defined as described in Equation 6.4, with the ratio R as given in Equation 6.3. For this the intensity I_{DA} of donor and acceptor is compared to that of the donor only I_D in its excited state. The change in the ratio R is later in the presence or absence of glucose is later on used to determine the effectiveness of the different sensors. The orientation factor κ, which is related to the angle between

the dipoles is relevant here. In order to understand the signal transfer κ and R_{DA} need to be known. In Equation 6.3 the transfer efficiency R is given and how it is related to the intensity of acceptor and donor FP. The change of R in the presence or absence of glucose is used to characterise sensor efficiency (see Figl 6.1 G-L).

6.3. Structural characterisation of variants with SAXS

In this section the SEC-SAXS results for sensors 1, 2, and 4 will be given. All experiments were performed as described in Section 4.3.2. The Kratky plots were compared for the sensors with and without glucose and the Guinier radii were calculated. By looking at the Guinier radii first, the change in sensor compactness over the whole ensemble can be accessed. This is an indication of whether or not the average relative FP distance changes drastically upon glucose addition. However, due to the axis symmetrical structure of the β-barrels no assumptions for κ can be made from these measurements.

The data analysed was that of the centre of the monomeric SEC elution peak and it was averaged over, as discussed in Section 4.3.3. When looking at a SEC elution profile it can be seen that one broad, one small, and a narrow high intensity peak are eluted in that order over time, see Fig. 6.4. Since smaller particles take longer to elute this indicates that the sample consisted of some aggregates, some higher order multimers, and the monomeric peak. All analysed SAXS data was measured from molecules of the monomeric peak.

The SAXS curves for the three selected sensors with and without glucose are shown in Fig. 6.5, as intensity vs. q and Kratky plots. It can be observed that the scattering curves measured for the sensors 1 and 4 do not change significantly upon glucose addition. This is different for sensor 2, where a difference between the glucose free and glucose bound state can be found in the plots. All curves were normalised to the intensity. The shape of the Kratky plots is indicative of a globular shape for all sensors.[94]

By performing a linear fit in the Guinier region of the Guinier plot, see Sections 3.2.2, 4.3.3, the Guinier radii were determined for the different sensors with and without

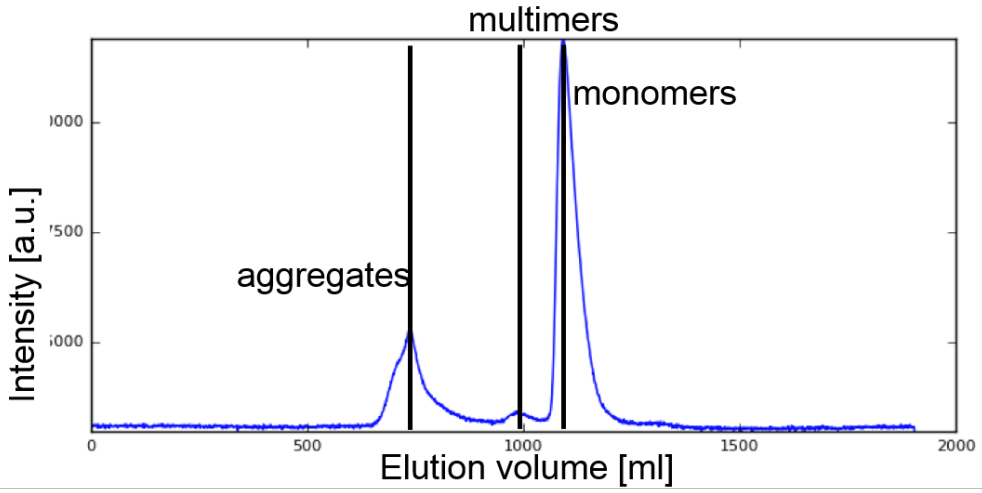

Figure 6.4.: *Representative SEC elution curve, here chosen for sensor 2 without glucose. The later a particle descends from the SEC column the smaller it is.*

glucose. The results are given in Table 6.1, with R_G being identical within the error for sensors 1 and 4 and reduced upon glucose binding for sensor 2. The reduction of the Guinier radius is indicative of an increased compactness of sensor 2 caused by glucose binding.

Table 6.1.: *The Guinier radii experimentally determined for the different sensors and calculated for Glc-BP. Sensors 1 and 4 are similar within the error. Sensor 2 shows a reduction of the Guinier radius upon glucose binding.*

sensor	$R_{G,\text{ no glucose}}$ [Å]	$R_{G,\text{ glucose}}$ [Å]	ΔR_G [Å]
sensor 1	38.73 ± 0.13	38.60 ± 0.48	0.16 ± 0.35
sensor 2	40.27 ± 0.71	37.91 ± 0.52	2.36 ± 0.19
sensor 4	40.42 ± 0.65	40.05 ± 0.35	0.37 ± 0.30
Glc-BP	22.84	21.73	1.11

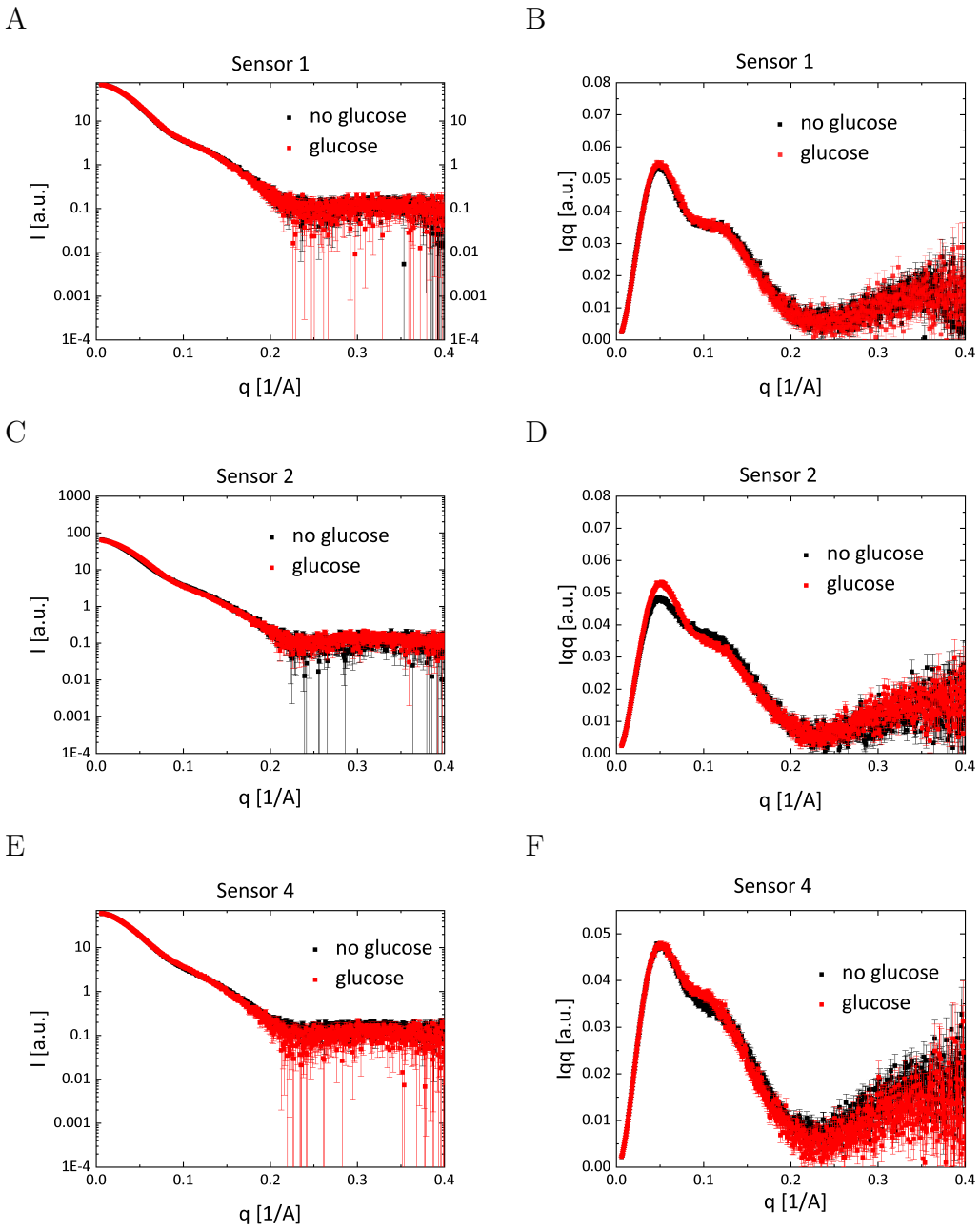

Figure 6.5.: *A, C, E show the scattered intensity plotted against the scattering vector q, while B, D, F show the Kratky plot for the same data. The black curves represent the respective sensors without glucose while the red curves represent the sensors with added glucose. A and B show the curves for sensor 1, C and D those for sensor 2,, and E and F those for sensor 4.*

6.4. Modelling of potential conformations

To create a first hypothesis of how the structure of the glucose sensors is affected by glucose binding, ensemble modelling to the SAXS data was performed. For this purpose the software EOM of the ATSAS package was used, as described in Section 4.3.3. Additional bead and rigid body models were created using DAMMIN, CORAL, and OLIGOMER, see Appendix E.

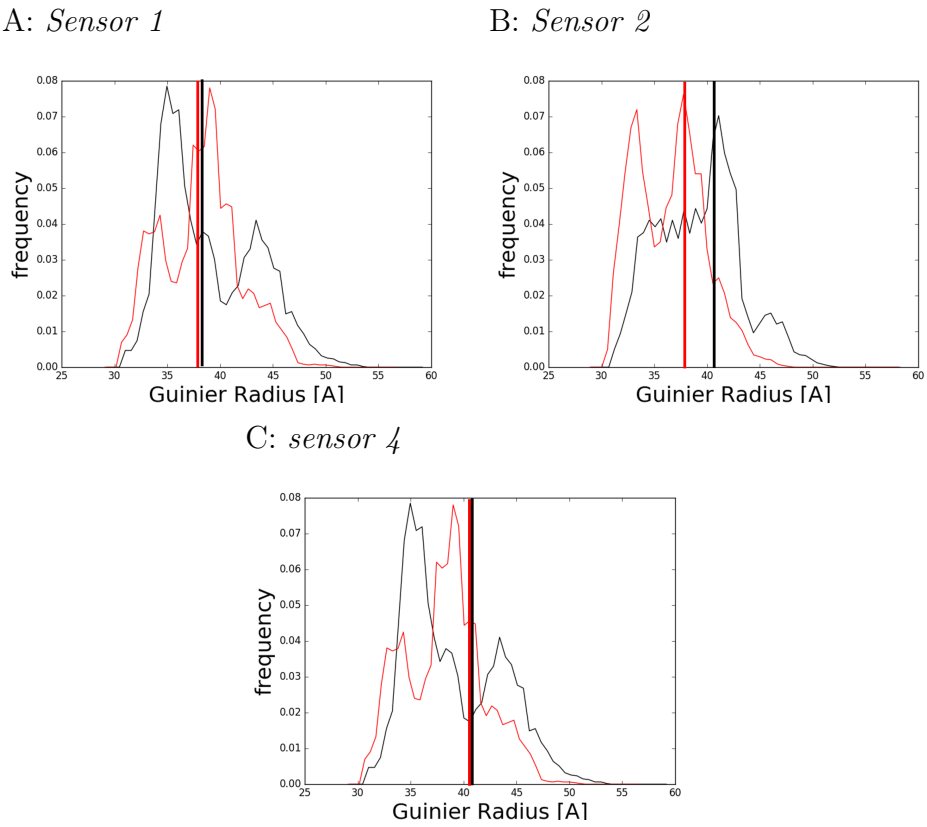

Figure 6.6.: *Ensemble models obtained with EOM with the results for added glucose being given in red and without glucose given in black. A shows the results for sensor 1, B for sensor 2, and C for sensor 4. In each case the probability of a different Guinier radius occurring in the ensemble is plotted against the Guinier radii. The lines indicate the experimentally determined Guinier radii.*

In order to gauge the different levels of compactness, which are likely to occur in the sensors with and without glucose, ensemble modelling was done using the software

	sensor 1	sensor 2	sensor 4
flexibility no glucose %	82.96	83.31	83.39
flexibility with glucose %	76.17	77.87	82.83
$R_{G,eom}^{noglucose}$ [Å]	38.46	39.48	39.46
$R_{G,eom}^{glucose}$ [Å]	36.06	36.93	38.42
$R_{G,exp}^{noglucose}$ [Å]	38.73 ± 0.13	40.27 ± 0.71	40.42 ± 0.65
$R_{G,exp}^{glucose}$ [Å]	38.60 ± 0.48	37.91 ± 0.52	40.05 ± 0.35

Table 6.2.: *Rigidity over ensembles for all sensors with and without glucose as obtained by EOM fits. Additionally the Guinier radii of the ensembles are given and for comparison purposes the experimental ones as well.*

EOM. 10,000 different geometrically accessible structures were created from the sub components of the different sensors, a more in depth description of how the software proceeded is given in Section 4.3.3. In Fig. 6.6 the probability of different Guinier radii being present in the ensemble is illustrated for each of the three sensors analysed with and without glucose present. For sensors 1, and 2 it can be observed that the flexibility is reduced upon glucose binding, see Table 6.2. For sensor 4 it does not change significantly between the glucose free and the glucose bound state. The average Guinier radii obtained by weighing their frequency within the ensembles are reduced upon glucose binding for sensors 1, and 2. However, they are not reduced as much for sensor 4, see Table 6.2. Both sensor 1 and 2 show two separate populations upon glucose binding, Fig. 6.6 (A), (B), although only sensor 1 also shows these for the glucose free state, where sensor 2 shows only one preferred population. Sensor 4 does not show distinct populations in either the glucose free or the glucose bound state.

When comparing the Guinier radii obtained with EOM to those obtained from the experiment it can be seen that EOM consistently underestimates the radii. Additionally it assumes a larger change of R_G for sensor 1 and 4 than actually occur. This suggests that additional constraints stop the sensors in solution from sampling all their geometrically possible states.

A comparison of the experimental data and the fit curves is shown in Fig. 6.7. Here it can be seen that while there is some deviant for $q > 0.35$ $\mathring{A}^{-1}$ for all sensors the

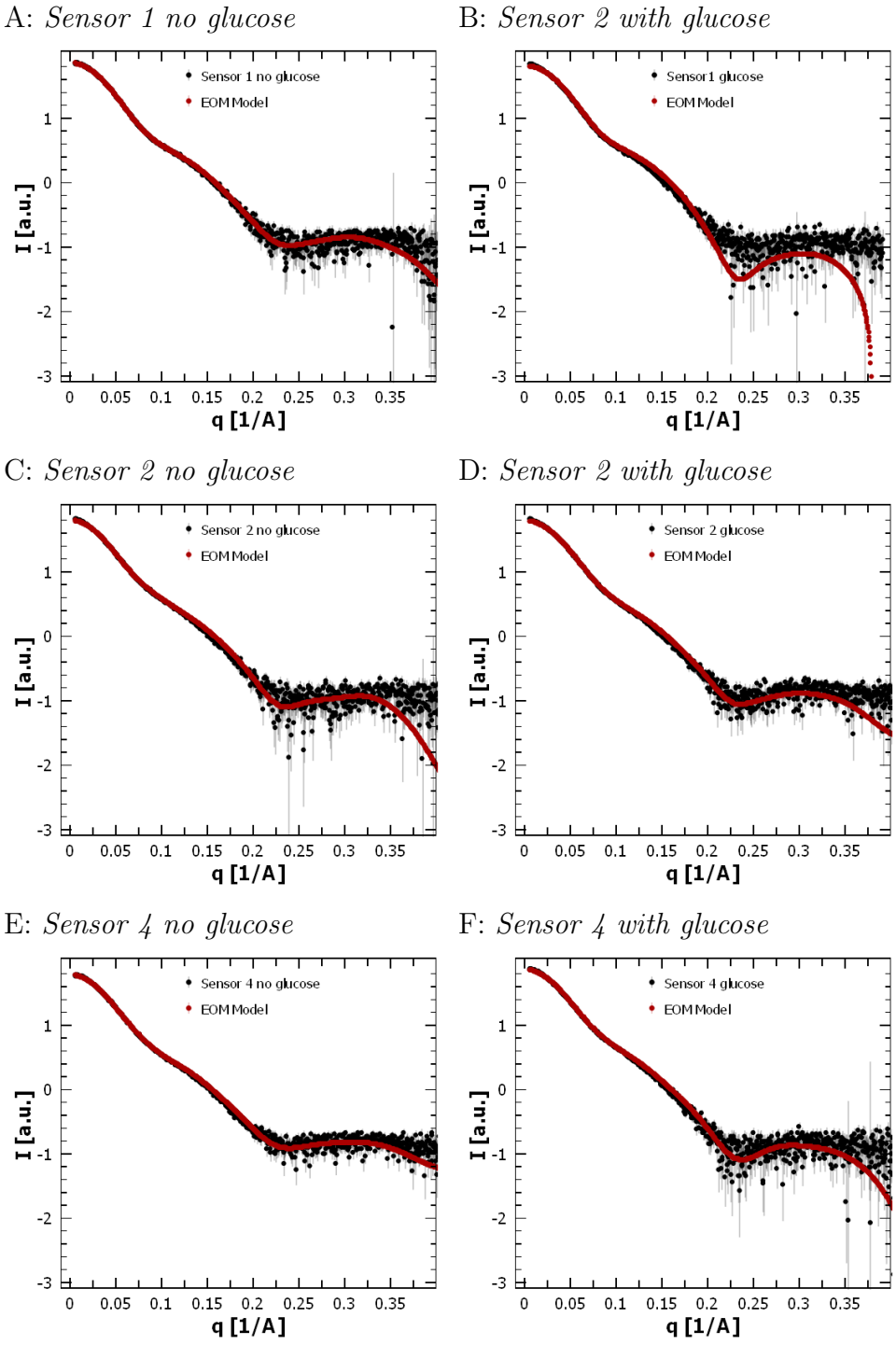

Figure 6.7.: *The experimental SAXS curves (black) plotted with the theoretical scattering curves for the EOM models (red) that describe them best. It can be observed that they show good agreement for low q but begin to deviate slightly around 0.35 Å^{-1}.*

fits otherwise agree reasonably well with the experimental data. A larger deviation is shown for sensor 1 with added glucose. This might be due of the lack of significant linkers in this construct. Therefore, reducing the flexibility of the sensor construct in solution more than anticipated in the modelling. For all sensor constructs the deviations at higher q are an indication of additional constraints being required to get a model with higher accuracy.

6.5. Discussion and Conclusion

The results obtained from the SAXS curves indicate that sensors 1 and 4 do not become more compact upon glucose binding, but rather remain the same. However, for sensor 2 glucose binding seems to cause an increase in the compactness, as indicated by the change in Guinier radii. This fits to the FRET data, which shows sensor 2 to have the largest change of the transfer rate between the glucose free and glucose bound state. Regarding the question of whether a change in FP distance, or solely a reorientation occurs, the Guinier radius is a good indicatior. Due to the axis symmetrical structure of the FPs, SAXS data cannot account for any potential rotational reorientations around this axis. For sensor 2 the Guinier radius is reduced, which supports the assumption that the change in signal transfer rate upon glucose binding is caused at least in part by a reduction of the relative FP distance. Since the SAXS data as it is, does not give any additional information, apart from the Guinier radius it is important to consider the information that can be obtained from the different models.

The bead models do not show a clearly resolved structure and thus cannot answer the question of how the sensor structure changes upon glucose binding. However, it can be used as a way to double check the rigid body models created. By plotting the rigid body models within the bead models a similarity between the structures can be seen. This, apart from the χ^2 values is a good indication that they describe the scattering data well. For the models found, two distinct subsets tend to appear, one where the FPs are far apart and one where they are quite close together. While each model on its own seems to fit the SAXS curve, a linear combination of the two gives a better fit, with the ratios as given in Fig. E.2, Table E.1. Since the sensor is assumed to be a very flexible structure, it is unlikely that a close approach of FPs would occur spontaneously for the time required to cause a FRET signal transfer, as the great flexibility of the structure would cause them to separate quite soon again. Neither is it likely to appear often enough to be a relevant part of the structures best describing the SAXS data based on current results. Therefore, it is likely that an additional constraint exists for the interaction of the sensor components that is as of yet not determined. Since FPs

have a tendency to stick together, it can be considered likely that the stickiness between the FPs used in the glucose sensor might stabilise the closed state.[95] While a mutated mTurquoise was used at the N-terminal, which did not include the area responsible for stickiness an unmutated Venus was used at the C-terminal.[95] Therefore, it is likely that the FPs kept their tendency to stick together if they approach closely, although it might have been reduced.

Since the rigid body models were only used to generate a small number of possible structures, the result from ensemble modelling also needs to be taken into consideration to account for the multiple configurations potentially present in solution. These models calculated the probability of different Guinier radii being present in the ensemble best describing the SAXS results, as well as the flexibility of the ensemble of structures that fits the data best.

The probability of the different Guinier radii for sensor 1 indicates that without glucose there is one distinct and one stretched clustering of conformations, Fig. 6.6 (A) black curve, while upon glucose addition, Fig. 6.6 (A) red curve, two distinct clusters occur. In addition to the emergence of a higher probability for two different Guinier radii clusters, it also becomes apparent that upon glucose addition a reduced Guinier radius is found to be more likely. This reduction is directly opposed to the experimental finding that the Guinier radius of sensor 1 does not change upon glucose addition. The most plausible explanation for this is the assumption that the exact probabilities being given for the different Guinier radii are not completely accurate. For this to be the case, the assumption must be made that an additional constraint apart from the geometric one caused by the linker structure exists. If additional constraints on the mobility or interaction of the FPs in relation to the glucose binding protein are introduced, the ratio of the clustered Guinier radii to each other might change. While this means that the ratio of the different clusters of Guinier radii to each other is not necessarily the one that will be present in solution, the two distinct populations are quite likely to be present. The flexibility appears to be reduced upon glucose addition, thus supporting the increased clustering around distinct Guinier radii, see Table 6.2.

For sensor 2 one distinct probability cluster of Guinier radii is found for the sensor without glucose, with the other Guinier radii appearing to be equally probable (see Fig. 6.6 B) black curve. Upon glucose addition (see Fig.6.6 B) red curve, two distinct clusters occur. This is coupled with an apparent reduction of the flexibility of sensor 2 upon glucose binding (see Table 6.2) which supports the increased clustering around distinct Guinier radii upon glucose binding. The total Guinier radius is also reduced upon glucose binding according to the ensemble model, which in this case fits with the SAXS data.

Sensor 4 shows no distinct probability clusters of the Guinier radii with or without glucose (Fig. 6.6 C). However, it also seems like there might be a slight preference for two different Guinier radii with and without glucose. Instead of sharp well defined peaks, the distribution is quite broad. Therefore, it is not appropriate to speak of clustering here. The Guinier radius is also not changed in the presence of glucose, fitting well to the SAXS data results. In addition, the flexibility of sensor 4 found by the ensemble modelling does not appear to change upon glucose binding and remains quite high.

The combined results from the rigid body modelling and ensemble modelling seem to suggest a configuration where the FPs are in a great distance from each other and one where they are close together. This observation seems to fit to the ensemble modelling results, where sensors 1 and 2 show similar changes in the probabilities of the different Guinier radii upon glucose addition, while sensor 4 behaves differently and does not show a clearly distinct change in behaviour.

Considering the results obtained from the modelling of the SAXS data and the SAXS data itself, as well as from regarding the FRET results, it becomes apparent that sensor 2 becomes more compact upon glucose binding. For sensor 1 and 4 a reduction of the distance between the FPs cannot be disregarded and is supported by the rigid body modelling. The ensemble modelling found that sensors 1 and 2 become more compact. By analysing which combination of the different structures are found with rigid body modelling fit the SAXS curves best, a linear combination of a state where the FPs are far apart and one where they are closer was found. For the different sensors the

ratio of these models and their individual configuration is of course not identical. This suggests that while the sensors are in solution and move freely without obtaining one static structure a very close approach of the FPs and one where they are quite far apart (see Fig. E.1) is the most likely state. However, the models do not only need to fit the SAXS data but also the FRET data in order to describe the sensor behaviour. As shown in Fig. 6.1 two different FRET populations were found for each sensor. When comparing this to the weighing of the models (see Table E.1) Sensor 2 is in qualitative agreement with the FRET data, as the majority of the population is shifted from less to more favourable. Opposed to this sensor 1 and sensor 4 do not agree. While the shift of sensor 1 is to complete sensor 4 does not shift enough. Further investigation of the potential conformations is therefore required.

For this purpose simulations which aim to fit the rigid body models they create to the SAXS data and then calculate the FRET efficiency for the created structures were performed by Ines Reinartz.[96] This cooperation resulted in additional models being created, which can now be taken into account for the interpretation of the sensor behaviour. When the modelling was performed without additional constraints the results for the sensors without glucose fit both the SAXS results and the FRET results well. However, for the glucose bound state the resulting models did not fit to the FRET results, rather they gave a far to low FRET efficiency, while still fitting the SAXS data. This suggests that without introducing additional constraints on the conformation and behaviour of the different sensor components, the FRET data cannot be explained. In order to see whether or not the results obtained for the ensemble model, where two distinct populations emerged for Sensors 1 and 2 upon glucose binding might be closer the separate models found from the modelling were analysed in more detail. The χ^2 of the modelled structures when compared to the SAXS curves was plotted against the FRET energy transfer of these structures. All structures which had a FRET energy transfer of sufficient height to explain the FRET results and a χ^2 below a threshold of 10 were marked in orange (see Fig. 6.8 A). When looking at these structures it becomes apparent that the FPs are quite close together, Fig. 6.8 B.

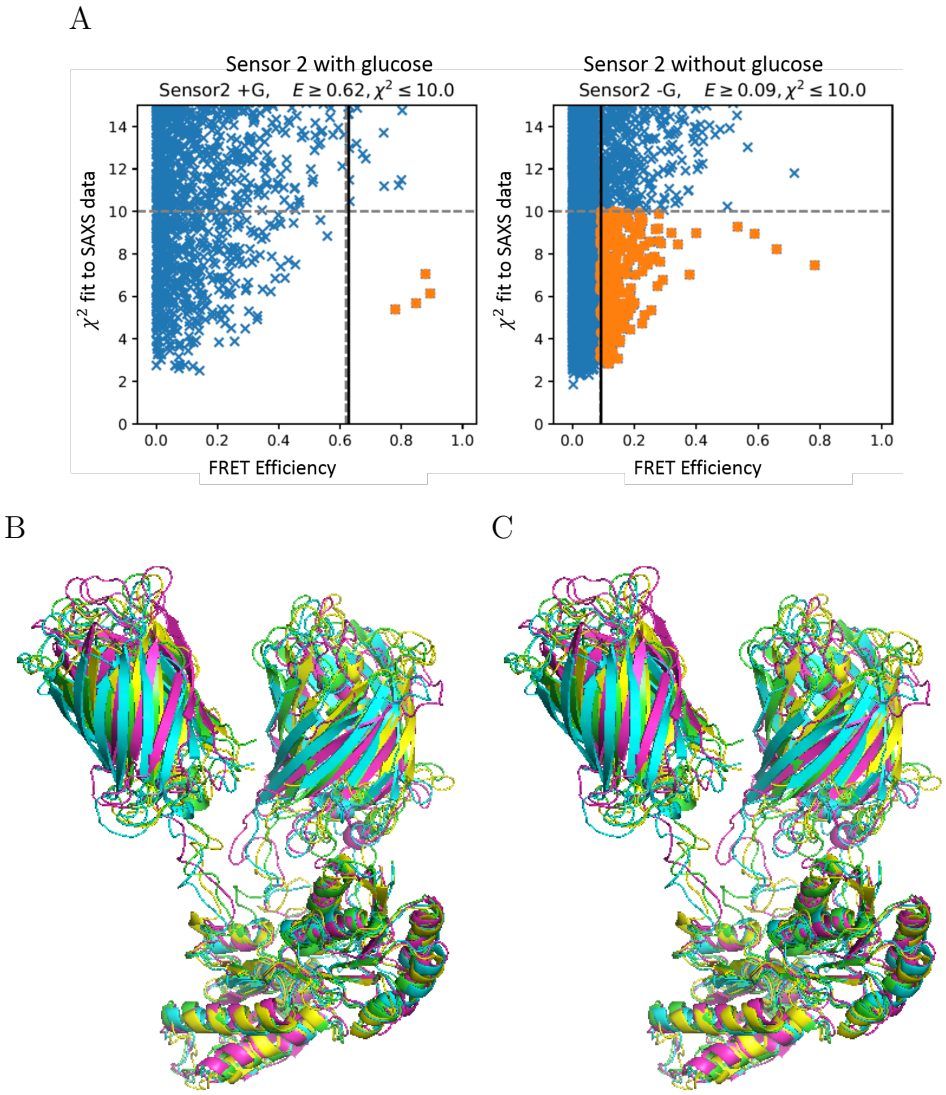

Figure 6.8.: *A shows the χ^2 of the model fit to SAXS data plotted against the FRET energy transfer for models simulated by Ines Reinartz for sensor 2.[96] Orange data points mark those that describe both the SAXS and FRET data well. B shows an example of those plots that fit the SAXS and FRET data for sensor 2 in the presence of glucose. This compact structure is unusual, as the rigid body models normally result in an open structure for sensor 2.*

These findings from the simulations done by Ines Reinartz lead to the conclusion that an additional constraint exists for the conformational orientation of the sensor components. This constraint is expected to increase the probability of the close approach of FPs upon glucose addition and explain why the introduction of an C-Terminal linker increases the FRET efficiency, while a N-Terminal linker reduces it. As the FPs are involved in this change the properties of the FPs come to mind as a potential source for the constraint. Therefore, it is plausible to assume that once the distance of the FPs falls below a certain threshold they do in fact stick together. This would allow for the close conformation and explain why no stable intermediate state between fully apart and close approach seems to exist.

While this assumption now accounts for the SAXS data and the FRET data, it does not offer an explanation on why the change in linkers affects the FRET efficiency. In order to answer this question mean distance between the FPs and how this changed with and without glucose binding for the different linkers was analysed. This can be done by looking at the average distance between the FPs during the simulations done by Ines Reinartz. Here it becomes apparent that the average distance is less for sensor 2 than for sensor 4, see Fig. 6.9. This could support the hypothesis of stickiness, as the reduced distance makes it more likely that the FPs approach close enough for this to occur, if an otherwise identical motion is assumed.

In conclusion it seems most likely that an ensemble of different structures explains the glucose sensor behaviour best and that the most efficient sensor, sensor 2, becomes on average more compact upon glucose binding. Simulations support that for the more efficient sensors an ensemble of structures with two clusters of structures being of higher probability is the most likely cause. These structures likely consist of an open structure and a more compact structure with the compact structure being due to the FPs stickiness. The probability of the compact structure, which causes the main FRET signal is most likely influenced by the linker position, as that affects the probability for the FPs to come into close proximity and therefore their probability to stick together.

While the combination of FRET and SAXS data with MD simulations did not give

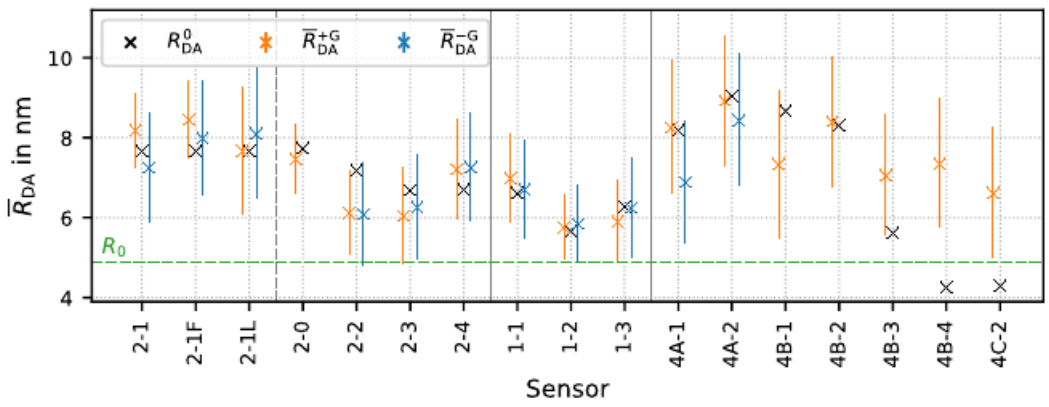

Figure 6.9.: *Distance between FPs in the presence and absence of glucose for the different sensors as obtained from a simulation done by Ines Reinartz.[96]*

a complete understanding of the causes behind the different FRET efficiencies of the sensor constructs it did allow for the formation of a hypothesis. Without the inclusion of the FRET data the models which fit the SAXS data well would have been deemed a sufficient explanation. By combining the results it becomes apparent that these models cannot provide the required FRET energy transfer.

6.6. Outlook

In order to be optimise the sensor construction the behavioural properties of a good sensor compared to one that does not perform as well need to be known. While the results presented here give a clear indication of an increase in sensor compactness being the cause of increased sensor efficiency a structural understanding has not been reached yet. In order to do this the additional unknown constraint required to find a structure, or an ensemble of structures, which fit the SAXS and FRET data needs to be isolated.

To verify or exclude the hypothesis of this constraint being caused by the stickiness of the sensors the experiments should be repeated with sensors where both FPs have, or do not have the mutation that prevents their interaction. By comparing the sensor performance in FRET and their SAXS curves the influence of these mutations could be

tested.

Additionally experiments to look at the structural changes of the sensor constructs in crowded conditions should be carried out, see Appendix F. For this purpose SANS experiments using a contrast matched crowding agent would be of use. As discussed in the appendix referenced above it will be important to ensure that no aggregation of oligomerisation of the sensor occurs. This could be achieved by performing multiple SEC experiments in order to establish the timescale on which the monomer does not aggregate. Before adding the Sensor to the crowded solution it would be run over a SEC and the SANS exposure limited to well below the time at which oligomerisation begins to occur.